Letter

Realization of an all-optical underdamped stochastic Stirling engine

Chuang Li,[1,*] Shaochong Zhu,[1,*] Peitong He,[1] Yingying Wang,[1] Yi Zheng,[1] Kexin Zhang,[1] Xiaowen Gao,[1,†] Ying Dong,[1,‡] and Huizhu Hu[1,2]

[1]*Research Center for Quantum Sensing, Intelligent Perception Research Institute, Zhejiang Lab, Hangzhou 311121, China*

[2]*State Key Laboratory of Modern Optical Instrumentation & College of Optical Science and Engineering, Zhejiang University, Hangzhou 310027, China*

(Received 7 June 2022; revised 30 March 2023; accepted 22 January 2024; published 26 February 2024)

We experimentally realize a nanoscale stochastic Stirling heat engine operating in the underdamped regime. The setup involves an optically levitated silica particle that is subjected to a power-varying optical trap and periodically coupled to a cold or hot reservoir via switching on or off of the active feedback cooling. We conduct a systematic investigation of the engine's performance and find that both the output work and efficiency approach their theoretical limits under quasistatic conditions. Furthermore, we examine the dependence of the output work fluctuation on the cycle time and the temperature difference between the hot and cold reservoirs. We observe that the distribution has a Gaussian profile in the quasistatic regime, whereas it becomes asymmetric and non-Gaussian as the cycle duration time decreases. This non-Gaussianity is qualitatively attributed to the strong autocorrelation of the particle's position within a cycle in the nonequilibrium regime. Our experiments provide valuable insights into stochastic thermodynamics in the underdamped regime and open up possibilities for the design of future nanomachines.

DOI: 10.1103/PhysRevA.109.L021502

Introduction. Thermodynamics deals with the relations between heat, work, temperature, entropy, and energy [1]. At its heart, is the heat engine, which converts heat to usable energy. Unlike its macroscopic counterpart that the deterministic classical thermodynamic laws can very well describe, a heat engine of micro or nanosize will undergo visible fluctuations [2], which makes it behave in a stochastic manner. In this regime, the central concepts of thermodynamics such as the exchanged heat, the applied work, and the entropy can be meaningfully defined on the level of individual trajectories [3,4]. These fluctuating quantities extend the laws of macroscopic thermodynamics and give birth to the so-called stochastic energetics [5]. With the advancement in the fabrication of microscopic mechanical devices, significant progress in the study of stochastic heat engines, both theoretical [6,7] and experimental [8,9], have been witnessed during the past decade.

A promising candidate for the experimental investigation of the stochastic thermodynamics [10–14] is the levitated optomechanical system (LOS) [15,16], where optical tweezers allow us to apply a fast and accurate control to the particle captured and record its spatial trajectory in real-time [17,18]. After a full description of a colloidal stochastic heat engine [19] given by Schmiedl and Siefert, Blickle and Bechinger realized a stochastic Stirling engine experimentally [20] for the first time. The efficiency of the Stirling engine is fundamentally limited by the isochoric steps, which make the cycle inherently irreversible. To overcome the limitations of the Stirling cycle, Martinez *et al.* implemented a Brownian Carnot cycle [21] with an optically trapped colloidal particle by creating an effective hot temperature bath with fluctuating electromagnetic fields, which allowed precise control over the bath temperature that is synchronized with the change of the trap stiffness and therefore a realization of an adiabatic ramp.

So far, the implementations of stochastic heat engines (SHEs) with a levitated microscopic particle are all in colloidal systems where the particle is overdamped [22,23]. The SHEs in the underdamped regime have been less investigated experimentally so far. We know that an analytic treatment of optimal protocols is possible in the overdamped case because the dynamics can be described by a simplified equation in terms of the slow position variable [19]. In contrast, this is not possible in the underdamped case, where the position and velocity variables cannot be separated. As a result, the optimization of an underdamped SHE for maximizing its performance is much more complicated than an overdamped one. Theoretical analysis showed that the rapid changes in the trapping frequency were desired to improve the power output and the efficiency [24]. More importantly, the investigations of much more isolated systems provide a path toward the future realization of quantum heat engines [25,26] or quantum refrigerators [27] in LOS and it has been shown that super Carnot efficiencies can be attained by clever reservoir engineering [28–30].

Inspired by a scheme [6] proposed by Dechant *et al.*, we present an experimental realization of an all-optical Stirling engine in the underdamped regime. The experimental setup is illustrated in Fig. 1(a). A charged silica particle of diameter 154.4 nm is levitated in a single-beam optical trap at the

*These authors contributed equally to this work.
†gaoxw@zhejianglab.com
‡yingdong@zhejianglab.com

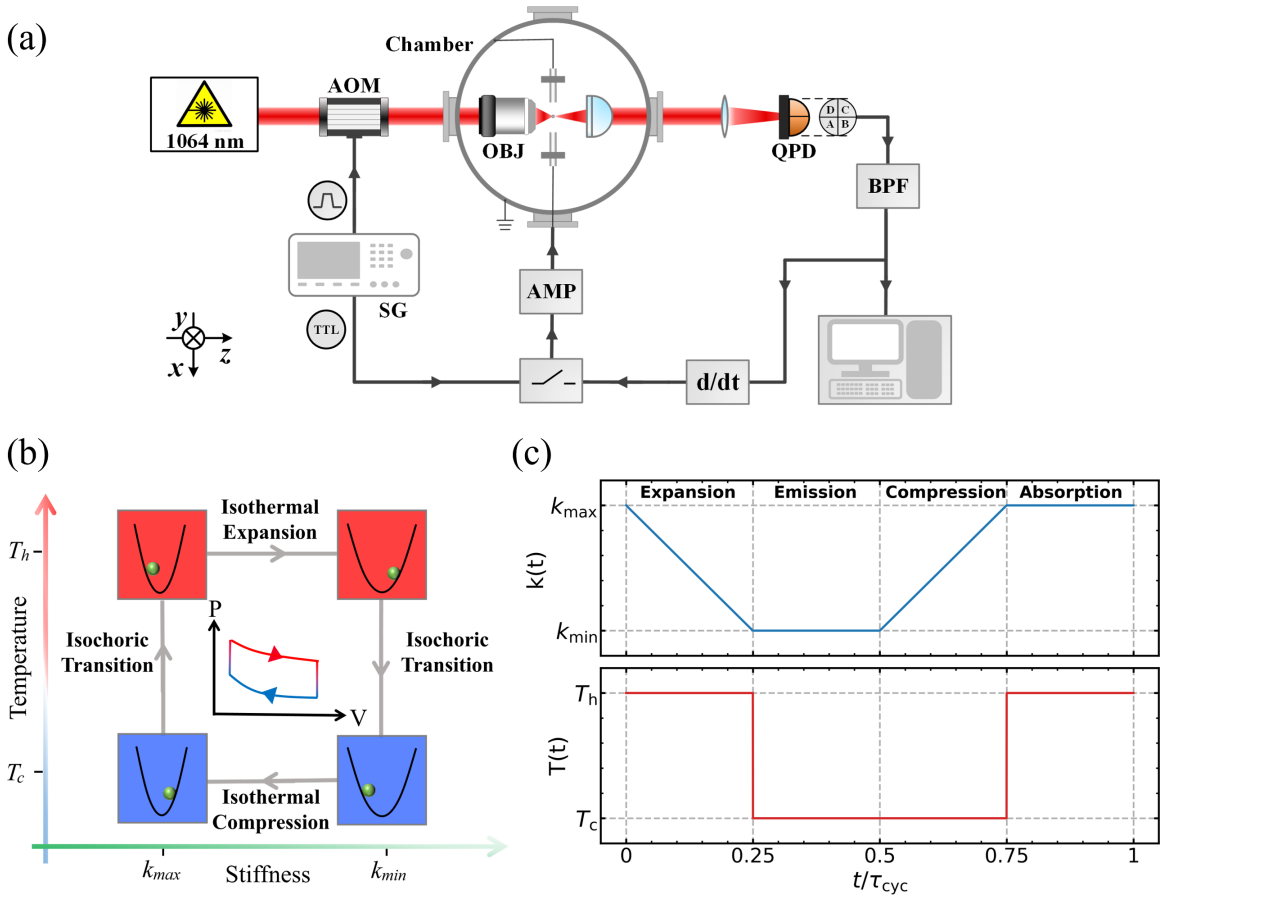

FIG. 1. (a) The experimental setup: A laser beam of wavelength 1064 nm passes an acoustooptic modulator (AOM) and is focused by a microscope objective (OBJ) with numerical aperture NA = 0.8 forming an optical trap, which levitates a charged silica particle inside a vacuum chamber. The trapping stiffness (or frequency) is dependent on the optical trapping power which can be changed by adjusting the driving voltage of the AOM. Throughout our work, we solely focus on the motion of the particle along the x axis. The scattered light from the particle is collected and sent to a quadrant photodetector (QPD) to detect the motion of the particle along the x axis. A feedback cooling scheme based on electric fields is applied to create the cold bath. In the scheme, the x-motion signal is sent through a bandpass filter (BPF) and a derivative circuit (d/dt) to provide a feedback signal proportional to velocity. This velocity-dependent feedback signal is sent to an amplifier (AMP) which modulates a pair of electrodes to cool the x motion electrically. To experimentally realize a stochastic Stirling cycle, we employ a signal generator (SG) that periodically outputs two synchronized signals. One signal is sent to the AOM to linearly change the optical trap power and the other one is sent to a switch to periodically turn on or off the feedback cooling. (b) The Stirling cycle consists of two isochoric and two isothermal strokes. The inset shows the analogy to a classical Stirling engine. (c) The optical trap stiffness $k(t)$ and the temperature of COM motion $T(t)$ as a function of time t during a Stirling cycle.

pressure of $p = 1.0$ mbar. The damping rate due to the collision with residual gas molecules is experimentally measured as $\Gamma_{\rm th}/2\pi = 1.45$ kHz. The optical potential is approximately harmonic with a power-dependent stiffness which therefore can be linearly tuned with an acoustooptic modulator (AOM). The resulting mechanical oscillation frequency of the particle $\Omega/2\pi$ ranges from 145.3 to 160.4 kHz. The surrounding gas environment coupling to the center of mass (COM) motion of the particle acts as the high-temperature reservoir (hot bath). The active feedback cooling, using electric fields to exert a force on the particle's motion and providing an additional feedback damping rate $\Gamma_{\rm fb}$, creates a controllable low-temperature reservoir (cold bath). A quadrant photodetector (QPD) monitors the motion of the particle so that its position trajectory can be accurately recorded. To realize a stochastic Stirling cycle consisting of two isothermal and two isochoric strokes, we employ a signal generator (SG) to periodically output two synchronized signals, which are inputted into the AOM to change the optical trap power and into the switch to turn on or off the feedback cooling, respectively. The details of the experimental setup and the protocol can be found in the caption of Fig. 1 and the Supplemental Material (SM) [31].

Model. As described above, the particle's oscillation frequency is much larger than the damping rate. Therefore, its COM motion is governed by the one-dimensional underdamped Langevin equation [32] (we solely focus on the particle's motion along the x axis throughout this work)

$$\dot{v} + \Gamma v + \frac{k(t)}{m}x = \sqrt{\frac{2k_B T\Gamma}{m}}\xi(t), \tag{1}$$

where m, x, and $v = \dot{x}$ respectively denote the mass, position, and velocity of the particle. $k(t) = m\Omega^2$ is the stiffness of the optical trap with the frequency Ω. $\Gamma = \Gamma_{\rm th} + \Gamma_{\rm fb}$ is the

total damping rate, T the effective COM temperature, and k_B the Boltzmann constant. The quantity $\xi(t)$ is a centered Gaussian white noise with $\langle \xi(t)\xi(t')\rangle = \delta(t-t')$. A Stirling cycle consisting of two isochoric and two isothermal strokes will be realized in the following steps.

(1) Expansion. Starting from the system in thermal equilibrium with the hot bath at the temperature T_h, it undergoes an isothermal expansion with stiffness $k(t)$ decreasing from k_{max} to k_{min} during a time duration τ_h. The particle keeps the connection to the hot reservoir via the coupling Γ_{th} during this stroke. To make sure that the stroke is isothermal, we require that the duration $\tau_h \gg 1/\Gamma_{th}$ and the oscillator therefore always equilibrates with the reservoir.

(2) Isochoric heat emission. The temperature of the reservoir is reduced to $T_c = \Gamma_{th}T_h/(\Gamma_{th}+\Gamma_{fd})$ by switching on the feedback cooling. In this stroke, the particle is instantaneously connected to the cold bath while the stiffness retains constant $k(t) = k_{min}$ lasting a time duration of τ_{hc} until its effective temperature of COM equilibrates to T_c.

(3) Compression. The system undergoes an isothermal compression with the stiffness $k(t)$ increasing back to k_{max} during a time duration τ_c. In this stage, the oscillator always keeps the connection to the cold bath at the constant temperature T_c.

(4) Isochoric heat absorption. The feedback cooling is switched off so that the particle is connected to the hot reservoir again and reaches back to the equilibrium state at the beginning of the cycle in a period of τ_{ch}. The stiffness keeps constant $k(t) = k_{max}$ during this stroke.

The total duration period of a cycle is then given by $\tau_{cyc} = \tau_h + \tau_{hc} + \tau_c + \tau_{ch}$. Here, we set the four strokes with the equal duration τ_s, i.e., the cycle time $\tau_{cyc} = 4\tau_s$. The schematic representation for a cyclic process of the Stirling engine and the changes of the trap stiffness and the effective COM temperature versus time are shown in Figs. 1(b) and 1(c), respectively.

One can draw an analogy between the particle in an optical trap and an ideal gas inside a piston, where the trap stiffness, or equivalently the trapping frequency, is analogous to the inverse of an effective volume while the variance of the particle position is seen as an effective pressure. Under this analogy, thermodynamic quantities can be extracted from the particle's positional fluctuations in the framework of stochastic thermodynamics. The total energy of the particle at time t reads

$$U(t) = \tfrac{1}{2}mv(t)^2 + \tfrac{1}{2}k(t)x(t)^2. \tag{2}$$

The increment of the energy dU can thus be divided into two parts where the work is defined as

$$dW = \frac{1}{2}\frac{dk}{dt}x^2 dt, \tag{3}$$

and the heat exchanged with the environment is defined as

$$dQ = mv\frac{dv}{dt}dt + kx\frac{dx}{dt}dt. \tag{4}$$

Integrating Eq. (3) along a stochastic trajectory yields the time-dependent work during a time duration $\tau = t_f - t_i$ as

$$W(\tau) = \frac{1}{2}\int_{t_i}^{t_f}\frac{dk(t)}{dt}x(t)^2 dt, \tag{5}$$

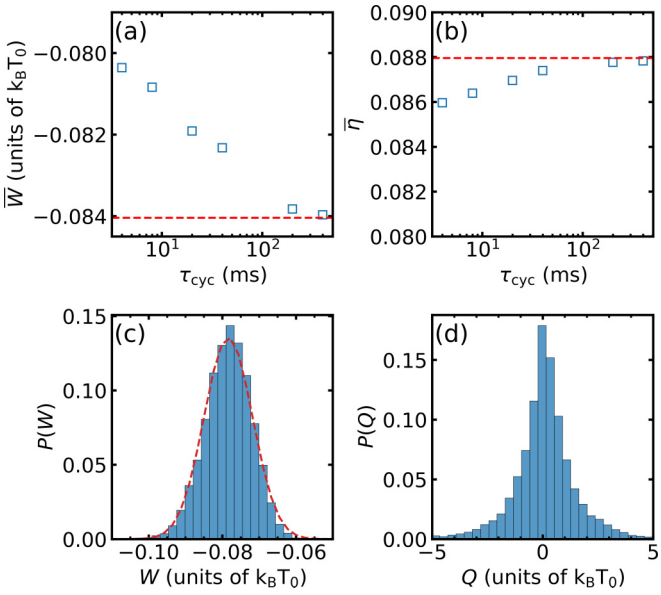

FIG. 2. (a) The mean output work $\overline{W}$ and (b) the mean efficiency $\overline{\eta} = -\frac{\overline{W}}{\overline{Q}}$ as a function of the cycle time τ_{cyc}. Here, the cycle time is chosen as $\tau_{cyc} = 4,\ 8,\ 20,\ 40,\ 200,\ 400$ ms. The red dashed lines in (a,b) are the theoretical values of the output work and efficiency in the quasistatic regime (see SM [31] for details), respectively. The probability distributions of (c) the output work W and (d) the absorbed heat Q in the quasistatic regime for the cycle time $\tau_{cyc} = 400$ ms. The red dashed line in (c) is a Gaussian distribution with the same mean and variance of the output work distribution. Throughout this paper, the work and the heat are all in units of k_BT_0. The temperature of the hot and the cold baths is experimentally determined as $T_h = 320$ K and $T_c = 65$ K, respectively. The number of Stirling cycles (ensemble number) in each experiment is fixed as $N = 10\,000$.

where t_i (t_f) is the initial (final) time. Meanwhile, the work W, heat Q, and inner energy U satisfy the stochastic first-law-like energy balance $\Delta U = W + Q$ for any single stochastic trajectory.

Experiments. We experimentally studied the performance of the Stirling engine in the underdamped regime. The optical stiffness linearly change in the range from $k_{min} = 3.21$ pN/μm ($\sim\Omega_{min}/2\pi = 145.3$ kHz) to $k_{max} = 3.92$ pN/μm ($\sim\Omega_{max}/2\pi = 160.4$ kHz). The effective COM temperature of the levitated particle is experimentally determined as $T_h = 320$ K and $T_c = 65$ K, respectively. Here, the temperature of the hot bath is a little bit larger than the room temperature $T_0 = 300$ K due to the heating effect of the trapping laser [33]. Figures 2(a) and 2(b) show the mean output work $\overline{W}$ and the mean efficiency $\overline{\eta} = -\frac{\overline{W}}{\overline{Q}}$ varying with the cycle time τ_{cyc}, respectively. The work and heat are both in units of k_BT_0 throughout this paper. One can see, both the mean output work $\overline{W}$ and the mean efficiency $\overline{\eta}$ monotonically increase with the cycle time and finally converge to the theoretical limit $\overline{W}_{qs} = -\frac{1}{2}\frac{T_h - T_c}{T_0}\ln\frac{k_{max}}{k_{min}}$ [34] and $\overline{\eta}_{qs} = \eta_c[1 + 2\eta_c/\ln(k_{max}/k_{min})]^{-1} \approx 0.088$, respectively, in the quasistatic regime with an infinite long cycle time. By the numerical simulations, we also figured out that the mean power $\overline{P} = -\frac{\overline{W}}{\tau_{cyc}}$ will reach its maximum value at $\tau_{cyc} \approx 0.04$ ms. It is not observed since 0.04 ms is much less than the shortest

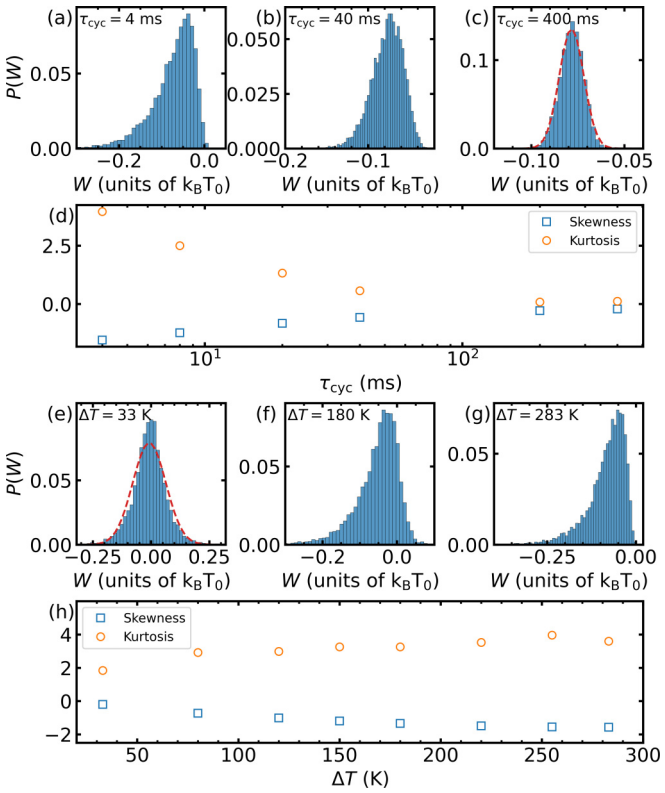

FIG. 3. (a)–(c) The probability distributions of the output work for the cycle time (a) $\tau_{cyc} = 4$ ms, (b) $\tau_{cyc} = 40$ ms, and (c) $\tau_{cyc} = 400$ ms (in the quasistatic regime). (d) The skewness and kurtosis as a function of the cycle time τ_{cyc}. In (a)–(d), the temperature difference between the hot and cold baths is fixed as $\Delta T = T_h - T_c = 255$ K. (e)–(g) The probability distributions of the output work for the temperature differences (e) $\Delta T = 33$ K, (f) $\Delta T = 180$ K, and (g) $\Delta T = 283$ K. (h) The skewness and kurtosis as a function of the temperature difference ΔT. In (e)–(h), the cycle time is fixed as $\tau_{cyc} = 4$ ms. The red dashed lines in (c) and (e) are the Gaussian distributions with the same mean and variance of the output work distribution.

cycle time $\tau_{cyc} = 4$ ms that is allowed in our experiments. The theoretical and simulation results and the detailed discussion of the power are presented in SM.

Figures 2(c) and 2(d) show the probability distributions of the output work W and the absorbed heat Q in the quasistatic regime for $\tau_{cyc} = 400$ ms. As expected, strong fluctuations can be seen in the output work and the absorbed heat. We compare the measured output work distribution with a Gaussian distribution with the same mean and variance in Fig. 2(c), which suggests that the output work distribution in the quasistatic regime is Gaussian.

We further explored the output work distribution for different cycle times, as shown in Figs. 3(a) to 3(c). Interestingly, we found that the profile of the work distribution becomes asymmetric (non-Gaussian) as we decrease the cycle time. Here, we introduce skewness and kurtosis to characterize the shapes of the work distributions. Figure 3(d) shows the skewness and kurtosis of the distributions versus the cycle time. The changing trends of them with the cycle time indicate that the output work deviates from the Gaussian distribution [34,35] when the engine operates under non-quasi-static conditions. From Fig. 3(a), we find that the output work distribution for $\tau_{cyc} = 4$ ms has an exponential tail. At the same time, the values of the skewness and kurtosis for $\tau_{cyc} = 4$ ms also indicate that this distribution is exponential. Likewise, the work distributions during both the expansion and compression strokes have an exponential tail (see SM), which is in good agreement with the theoretical prediction in the underdamped regime [35].

Moreover, we find that the work distribution profile also depends on the temperature difference $\Delta T = T_h - T_c$ between the hot and cold baths. Figures 3(e) and 3(g) show how the work distribution changes with varying the temperature difference ΔT for the short cycle time $\tau_{cyc} = 4$ ms, and the skewness and kurtosis versus the temperature difference is plotted in Fig. 3(h). The results show that the work distribution with a short cycle time can change from asymmetric to symmetric with decreasing temperature differences. However, the symmetric distribution (skew $\to 0$) is still non-Gaussian with a nonzero kurtosis. In addition, in the case of a small temperature difference, our experiment successfully verified the Jarzynski equality [36,37] and the Crooks equation [38] (see SM for details).

Discussions and conclusion. The position of an oscillator driven by a random Brownian force is a random variable. In the quasistatic regime, the equipartition theorem states that the stochastic position at different instants should be a Gaussian-distributed random variable with the variance $\langle x^2(t)\rangle = k_B T/k(t)$. Figure 4(a) shows the position variance $\langle x^2(t)\rangle$ (ensemble average) versus time during a cycle in the quasistatic regime, and the inset shows the measured position distribution at different instants. They agree well with the prediction from the equipartition theorem. As a result, the output work W calculated via Eq. (5) would be the integration (or sum) of squares of a series of Gaussian-distributed random variable $x(t)$. It is well known that, for a large number of independent random variables with an arbitrary but identical distribution, the sum of them will tend toward a Gaussian distribution. However, the distributions of $x^2(t)$ at different instants are obviously not the same for the varying stiffness $k(t)$. To understand the work distribution observed in the experiments, we numerically investigate the distribution of the sum of the squares of a sequence of independent Gaussian random variables $\{X_1, X_2, \ldots, X_{2N}\}$ with zero mean $\langle X_i\rangle = 0$ and varying variance $\langle X_i^2\rangle = T_i/k_i$, where T_i and k_i are two independent parameters, respectively. An analogy to the isothermal strokes in the Stirling cycle, we set T_i to be constant while k_i scale linearly with i, i.e., $T_i = 1$, $k_i = \frac{(\beta-1)i+N-\beta}{N-1}$ for $i \leqslant N$ and $T_i = \alpha$, $k_i = \frac{1-\beta}{N} i + 2\beta - 1$ for $N < i \leqslant 2N$, where $\alpha = \frac{T_c}{T_h}$ and $\beta = \frac{k_{min}}{k_{max}}$ denote the temperature ratio and the stiffness ratio, respectively. Figure 4(b) shows the distribution of the square sum $Y = \sum_i^{2N} X_i^2$ for the same stiffness and temperature in Fig. 3(c), which indicates that the sum of the squares of a sequence of independent Gaussian-distributed random variables with varying variances is still a Gaussian random variable and explains the experimental results we observed under the quasistatic condition.

As the cycle time decreases, the equipartition theorem is no longer held due to the fast-varying stiffness. In this situation,

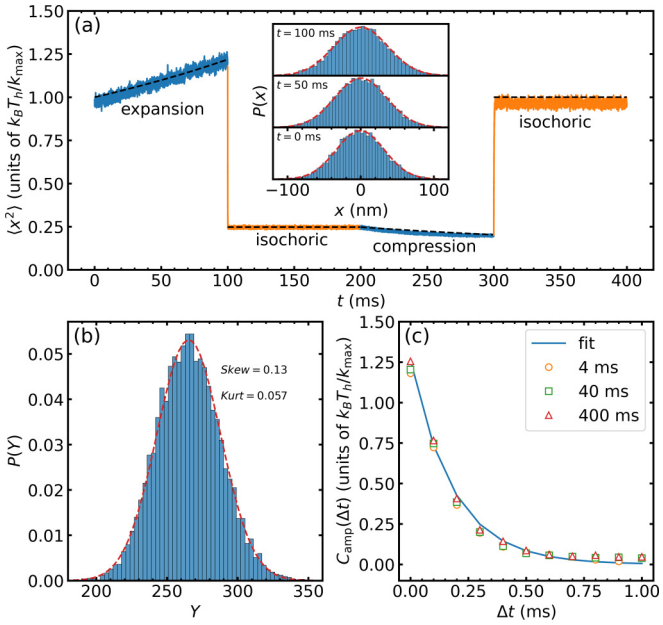

FIG. 4. (a) The position variance $\langle x^2(t)\rangle$ (ensemble average) versus time during a cycle in the quasistatic regime for $\tau_{\rm cyc} = 400$ ms, and the inset shows the measured position distributions at different instants $t = 0,\ 50,\ 100$ ms. The black dashed lines are the theoretical prediction of $\langle x^2(t)\rangle$ according to the equipartition theorem. The comparison of the position variance varying between the quasistatic and nonequilibrium cases is shown in SM. (b) The distribution of the sum of squares of random variables $Y = \sum_i X_i^2$. Here, the red dashed line is a Gaussian distribution with the same mean and variance of the distribution. The skewness and kurtosis are also labeled in (b). (c) The amplitude of the position correlation function $C_{\rm amp}(\Delta t)$ in units of $k_B T_h/k_{\rm max}$ for different cycle times.

not only is the consistency of the distribution disrupted, but so is the independence of the variables. We calculate the autocorrelation function (ACF) $C(t, t+\Delta t) = \langle x(t)x(t+\Delta t)\rangle$ of the particle displacement during the expansion stroke. For a given Δt, the ACFs oscillate in the time domain with an amplitude $C_{\rm amp}(\Delta t)$ (see SM for details). As shown in Fig. 4(c), the amplitudes $C_{\rm amp}(\Delta t) \propto e^{-\frac{\Delta t}{t_{\rm corr}}}$ decays exponentially with a characteristic correlation time $t_{\rm corr} \simeq 0.2$ ms for all different cycle times. Since $t_{\rm corr}$ is comparable to the duration of the expansion (compression) stroke which is 1 ms in the case of rapid stiffness variation, we can expect that the correlation between the particle's positions at different instants will play an important role and lead to the non-Gaussian distributed output work.

In summary, we experimentally realize a nanosized stochastic Stirling engine based on a levitated optomechanical system, where a silica particle serving as the working medium is subjected to the power-varying optical tweezers and coupled periodically to the cold (hot) reservoir created by switching on (off) feedback cooling. The experimental performance of the Stirling cycles including the work, heat, and efficiency is presented. Our experimental results show that the output work distribution of the underdamped stochastic Stirling engine is Gaussian in the quasistatic regime, and it becomes more and more non-Gaussian as the cycle time decreases. This non-Gaussianity is qualitatively attributed to the strong correlation of the particle's position within a cycle in the nonequilibrium regime. Unfortunately, the exact probability distribution function of the output work for a fast stiffness variation in the underdamped regime is yet unknown [14].

The experimental study on the SHE in the underdamped regime has just begun. There are still a lot of open questions waiting to be answered. In this sense, the present work can be regarded as a preliminary exploration in this field. In the following, with an upgraded electronic controlling system, more complex investigations of the underdamped SHE such as the optimal efficiency at the max power, or dynamical behaviors of Otto cycles and Carnot cycles will be further explored. Integrating with the ground-state cooling [39–41] techniques demonstrated recently, our system could be directly turned into the platform for investigating real quantum mechanical nanomachines.

Acknowledgments. This work is supported by the Major Scientific Research Project of Zhejiang Lab (2019 MB0AD01), the Center Initiated Research Project of Zhejiang Lab (Grant No. 2021MB0AL01), National Natural Science Foundation of China (Grant No. 12304545), and Zhejiang Provincial Natural Science Foundation of China (Grant No. LQ22A040010). X.G acknowledges support from the Research Project for Young Scientists of Zhejiang Lab (Grant No. 2020MB0AA04), Zhejiang Laboratory Research Found (Grant No. 2021MB0AL02), and the Major Project of Natural Science Foundation of Zhejiang Province (Grant No. LD22F050002).

[1] E. Fermi, *Thermodynamics*, New ed. (Dover, New York, 2000).
[2] R. E. Spinney and I. J. Ford, Fluctuation relations: A pedagogical overview, in *Nonequilibrium Statistical Physics of Small Systems* (Wiley-VCH, Weinheim, 2013), Chap. 1, pp. 3–56.
[3] U. Seifert, Entropy production along a stochastic trajectory and an integral fluctuation theorem, Phys. Rev. Lett. **95**, 040602 (2005).
[4] U. Seifert, Stochastic thermodynamics, fluctuation theorems and molecular machines, Rep. Prog. Phys. **75**, 126001 (2012).
[5] K. Sekimoto, *Stochastic Energetics*, 1st ed., (Springer, Berlin, 2010).
[6] A. Dechant, N. Kiesel, and E. Lutz, All-optical nanomechanical heat engine, Phys. Rev. Lett. **114**, 183602 (2015).
[7] Y. Dong, K. Zhang, F. Bariani, and P. Meystre, Work measurement in an optomechanical quantum heat engine, Phys. Rev. A **92**, 033854 (2015).
[8] S. Ciliberto, Experiments in stochastic thermodynamics: Short history and perspectives, Phys. Rev. X **7**, 021051 (2017).

[9] J. Sheng, C. Yang, and H. Wu, Realization of a coupled-mode heat engine with cavity-mediated nanoresonators, Sci. Adv. **7**, eabl7740 (2021).

[10] J. Gieseler, L. Novotny, and R. Quidant, Thermal nonlinearities in a nanomechanical oscillator, Nat. Phys. **9**, 806 (2013).

[11] J. Gieseler, R. Quidant, C. Dellago, and L. Novotny, Dynamic relaxation of a levitated nanoparticle from a non-equilibrium steady state, Nat. Nanotechnol. **9**, 358 (2014).

[12] L. Rondin, J. Gieseler, F. Ricci, R. Quidant, C. Dellago, and L. Novotny, Direct measurement of Kramers turnover with a levitated nanoparticle, Nat. Nanotechnol. **12**, 1130 (2017).

[13] J. Gieseler and J. Millen, Levitated nanoparticles for microscopic thermodynamics—A review, Entropy **20**, 326 (2018).

[14] M. Rademacher, M. Konopik, M. Debiossac, D. Grass, E. Lutz, and N. Kiesel, Nonequilibrium control of thermal and mechanical changes in a levitated system, Phys. Rev. Lett. **128**, 070601 (2022).

[15] J. Millen, T. S. Monteiro, R. Pettit, and A. N. Vamivakas, Optomechanics with levitated particles, Rep. Prog. Phys. **83**, 026401 (2020).

[16] C. Gonzalez-Ballestero, M. Aspelmeyer, L. Novotny, R. Quidant, and O. Romero-Isart, Levitodynamics: Levitation and control of microscopic objects in vacuum, Science **374**, eabg3027 (2021).

[17] A. Ashkin and J. Dziedzic, Optical levitation in high vacuum, Appl. Phys. Lett. **28**, 333 (1976).

[18] A. Ashkin, J. M. Dziedzic, J. E. Bjorkholm, and S. Chu, Observation of a single-beam gradient force optical trap for dielectric particles, Opt. Lett. **11**, 288 (1986).

[19] T. Schmiedl and U. Seifert, Efficiency at maximum power: An analytically solvable model for stochastic heat engines, Europhys. Lett. **81**, 20003 (2008).

[20] V. Blickle and C. Bechinger, Realization of a micrometre-sized stochastic heat engine, Nat. Phys. **8**, 143 (2012).

[21] I. A. Martínez, É. Roldán, L. Dinis, D. Petrov, J. M. Parrondo, and R. A. Rica, Brownian Carnot engine, Nat. Phys. **12**, 67 (2016).

[22] A. Imparato, L. Peliti, G. Pesce, G. Rusciano, and A. Sasso, Work and heat probability distribution of an optically driven Brownian particle: Theory and experiments, Phys. Rev. E **76**, 050101(R) (2007).

[23] I. A. Martinez, É. Roldán, L. Dinis, and R. A. Rica, Colloidal heat engines: a review, Soft Matter **13**, 22 (2017).

[24] A. Dechant, N. Kiesel, and E. Lutz, Underdamped stochastic heat engine at maximum efficiency, Europhys. Lett. **119**, 50003 (2017).

[25] K. Zhang, F. Bariani, and P. Meystre, Quantum optomechanical heat engine, Phys. Rev. Lett. **112**, 150602 (2014).

[26] K. Zhang, F. Bariani, and P. Meystre, Theory of an optomechanical quantum heat engine, Phys. Rev. A **90**, 023819 (2014).

[27] Y. Dong, F. Bariani, and P. Meystre, Phonon cooling by an optomechanical heat pump, Phys. Rev. Lett. **115**, 223602 (2015).

[28] J. Roßnagel, O. Abah, F. Schmidt-Kaler, K. Singer, and E. Lutz, Nanoscale heat engine beyond the Carnot limit, Phys. Rev. Lett. **112**, 030602 (2014).

[29] J. Klaers, S. Faelt, A. Imamoglu, and E. Togan, Squeezed thermal reservoirs as a resource for a nanomechanical engine beyond the Carnot limit, Phys. Rev. X **7**, 031044 (2017).

[30] W. Niedenzu, V. Mukherjee, A. Ghosh, A. G. Kofman, and G. Kurizki, Quantum engine efficiency bound beyond the second law of thermodynamics, Nat. Commun. **9**, 165 (2018).

[31] see Supplemental Material at http://link.aps.org/supplemental/10.1103/PhysRevA.109.L021502 for the details of the experimental setup and the protocol.

[32] E. Aurell, On work and heat in time-dependent strong coupling, Entropy **19**, 595 (2017).

[33] J. Millen, T. Deesuwan, P. Barker, and J. Anders, Nanoscale temperature measurements using non-equilibrium Brownian dynamics of a levitated nanosphere, Nat. Nanotechnol. **9**, 425 (2014).

[34] S. Rana, P. S. Pal, A. Saha, and A. M. Jayannavar, Single-particle stochastic heat engine, Phys. Rev. E **90**, 042146 (2014).

[35] C. Kwon, J. D. Noh, and H. Park, Work fluctuations in a time-dependent harmonic potential: Rigorous results beyond the overdamped limit, Phys. Rev. E **88**, 062102 (2013).

[36] C. Jarzynski, Nonequilibrium equality for free energy differences, Phys. Rev. Lett. **78**, 2690 (1997).

[37] C. Jarzynski, Equilibrium free-energy differences from nonequilibrium measurements: A master-equation approach, Phys. Rev. E **56**, 5018 (1997).

[38] G. E. Crooks, Entropy production fluctuation theorem and the nonequilibrium work relation for free energy differences, Phys. Rev. E **60**, 2721 (1999).

[39] U. Delić, M. Reisenbauer, K. Dare, D. Grass, V. Vuletić, N. Kiesel, and M. Aspelmeyer, Cooling of a levitated nanoparticle to the motional quantum ground state, Science **367**, 892 (2020).

[40] L. Magrini, P. Rosenzweig, C. Bach, A. Deutschmann-Olek, S. G. Hofer, S. Hong, N. Kiesel, A. Kugi, and M. Aspelmeyer, Real-time optimal quantum control of mechanical motion at room temperature, Nature (London) **595**, 373 (2021).

[41] F. Tebbenjohanns, M. L. Mattana, M. Rossi, M. Frimmer, and L. Novotny, Quantum control of a nanoparticle optically levitated in cryogenic free space, Nature (London) **595**, 378 (2021).